Acta Montanistica Slovaca
ISSN 1335-1788
actamont.tuke.sk

Determining the accuracy of SLAM and SLAM GNSS-RTK scanning for monitoring earthworks

Tomáš KŘEMEN[1], Martin ŠTRONER[2], Rudolf URBAN[3], Jaroslav BRAUN[4]* and *Alice ADAMCOVÁ[5]*

Authors' affiliations and addresses:
[1] Department of Special Geodesy, Faculty of Civil Engineering, Czech Technical University in Prague, Thákurova 7, 166 36 Prague 6, Czech Republic e-mail: tomas.kremen@fsv.cvut.cz

[2] Department of Special Geodesy, Faculty of Civil Engineering, Czech Technical University in Prague, Thákurova 7, 166 36 Prague 6, Czech Republic e-mail: tomas.kremen@fsv.cvut.cz

[3] Department of Special Geodesy, Faculty of Civil Engineering, Czech Technical University in Prague, Thákurova 7, 166 36 Prague 6, Czech Republic e-mail: tomas.kremen@fsv.cvut.cz

[4] Department of Special Geodesy, Faculty of Civil Engineering, Czech Technical University in Prague, Thákurova 7, 166 36 Prague 6, Czech Republic e-mail: tomas.kremen@fsv.cvut.cz

[5] Department of Special Geodesy, Faculty of Civil Engineering, Czech Technical University in Prague, Thákurova 7, 166 36 Prague 6, Czech Republic e-mail: tomas.kremen@fsv.cvut.cz

***Correspondence:**
Tomáš Křemen, Department of Special Geodesy, Faculty of Civil Engineering, Czech Technical University in Prague, Thákurova 7, 166 36 Prague 6, Czech Republic tel.: +420-22435-4668 e-mail: tomas.kremen@fsv.cvut.cz s

Funding information:
European Union project
CZ.02.01.01/00/23_020/0008487
Technology Agency of The Czech Republic
SQ01010105.

Acknowledgement:
The research was co-funded by the European Union under the project INODIN, no. CZ.02.01.01/00/23_020/0008487 and The Technology Agency of The Czech Republic under the project MESVYVED no. SQ01010105.

How to cite this article:
Křemen, T., Štroner, M., Urban, R., Braun, J. and Adamcová, A. (2025). Determining the accuracy of SLAM and SLAM GNSS-RTK scanning for monitoring earthworks. *Acta Montanistica Slovaca*, Volume 30 (4), 934-946

DOI:
https://doi.org/10.46544/AMS.v30i4.08

Abstract
This study evaluates the accuracy of SLAM-based LiDAR scanning and SLAM integrated with GNSS-RTK for monitoring large-scale earthworks. The experiment was conducted on a soil deposit created during motorway construction in Central Bohemia, measuring approximately 150 m × 55 m × 15 m. A Leica P40 terrestrial laser scanner served as the reference system, producing a high-precision point cloud georeferenced via ground control points (GCPs). The tested system, Emesent Hovermap ST-X, was deployed in two configurations: (i) georeferencing using GCPs and (ii) trajectory determination via a continuously connected GNSS-RTK receiver mounted on the scanning backpack. Data processing involved point cloud registration, smoothing using Moving Least Squares, and accuracy assessment through root mean square deviation (RMSD) analysis against the reference dataset. Four SLAM point clouds were acquired—two using GCPs and two using GNSS-RTK—along with their smoothed variants. Results indicate that GCP-based georeferencing achieved RMSD values around 17 mm, closely matching the manufacturer's declared mapping accuracy of 15 mm. GNSS-RTK-based measurements yielded slightly higher RMSD values (≈20 mm), which remain within acceptable limits given the inherent GNSS-RTK positional accuracy (10 mm horizontally, 40 mm vertically). Systematic height shifts were observed in RTK datasets, emphasizing the need for minimal control points to correct vertical bias.
The findings confirm that SLAM scanning is a more practical alternative to static terrestrial scanning for earthwork monitoring, significantly reducing operational complexity and time. While GCP-based workflows deliver optimal accuracy, GNSS-RTK integration offers a faster solution with minor trade-offs in vertical precision. Proper route planning and strategic GCP placement are critical for achieving manufacturer-specified accuracy, particularly in areas with limited connectivity between scanned surfaces. Overall, both approaches provide sufficient precision for engineering applications, with RMSD values ≤25 mm, validating SLAM technology as an efficient tool for large-scale geospatial monitoring.

Keywords
SLAM, GNSS_RTK, earthworks, 3D scanning, accuracy testing

Introduction

In recent years, laser scanning has become one of the main methods for surveying the actual state across scientific disciplines, e.g., construction (Antova, 2024), (Dragomir et al., 2025), (Chen et al., 2025), forestry (Muhojoki et al., 2024), (Eker et al., 2022), mining (Singh et al., 2022), (Janus et al., 2022), (Kovanič, 2013), geotechnical and geological surveys (Pukanská et al., 2024), (Kovanič et al., 2024), heritage conservation (Liu et al., 2023), (Rocha et al., 2024) and many others.

Advances in this technology already allow scanning systems to be mounted not only on various static platforms, but also on mobile platforms such as cars (Kalenjuk et al., 2022), (Issaoui et al., 2021), UAVs (Del Carmen Vílchez-Lara et al., 2024), (Bartmiński et al., 2022), ships (Pei et al., 2021), (Flener et al., 2013), and fully robotic systems (Koszyk et al., 2023), (Fortuna et al., 2025). The use of scanners that work with SLAM (Simultaneous Localization and Mapping) technology has become a significant milestone across many types of work. Although these scanners do not yet achieve the same accuracy as static scanners, they have the enormous advantage of high data collection efficiency and coverage, as shown, for example, in the article (Štroner et al., 2024).

Determining the correct trajectory of movement is crucial for the proper functioning of SLAM scanners. This trajectory is primarily determined from the scanned objects themselves, and it is therefore advisable to choose an environment that contains distinct geometric features, which is usually the case with interiors (Gharebaghi et al., 2021), (Jiang et al., 2024), (Emmanouil et al., 2025), but also some types of exteriors (Běloch & Pavelka, 2025), (Chudá et al., 2024). If there is a shortage of such features, SLAM slip may occur, or the trajectory may be lost altogether, resulting in scanning failure.

In most commercial systems, the movement trajectories can be further processed by GCPs (Ground Control Points) determined, for example, using a total station, where it is possible to place the scanner directly on the GCP (Faro Orbis) or select these GCPs directly from the scanned data during subsequent processing (Emesent Hoovermap). Testing of SLAM scanners using GCPs was carried out, for example, in (Křemen et al., 2024), where the authors investigated the use of the Emesent Hovermap ST-X SLAM scanner in an underground environment at a very long distance of 750 m, and the accuracy of the system ranged from 5 to 8 cm with two (recommended) passes. In urban areas (Kovanič et al., 2025), the accuracy of mobile systems using GCPs was around 3 cm for Lidaretto and around 2 cm for Stonex X120GO. In a similar study (Maset et al., 2025), the Stonex system also achieved an accuracy of 2 to 5 cm for the height component. A study (Chrbolková et al., 2025) in a more extensive test of various SLAM scanners in an industrial building reported accuracies of around 1 cm for the Faro Orbis and Emesent Hovermap SLAM scanners. In a large surface quarry environment, Faro Orbis was tested (Kovanič et al., 2025b) using GCP, with an accuracy of around 3 cm. The accuracy of the Livox Avia SLAM scanner clouds compared to data from the Riegl VZ-400i static scanner for various buildings is reported in a study (Szrek et al., 2024), where the calculated RMSE value is 5 cm. For scanning a bridge structure with the ZEB Horizon SLAM scanner, an accuracy of around 5 cm is also reported in (Urban et al., 2024). The accuracy of SLAM systems using GCP is, therefore, relatively sufficiently tested.

A completely different approach to trajectory determination for outdoor use is offered by SLAM scanners, which can be combined with a GNSS RTK receiver. Theoretically, this completely eliminates the time-consuming surveying and GCP installation, further increasing the efficiency of these scanners.

In view of the statements above, the article aims to test the accuracy of the measurement results of a SLAM scanner with a trajectory determined using the GNSS RTK method, in comparison with significantly more accurate terrestrial scanning performed by a static Leica P40 scanner with millimeter accuracy, but also with the measurement results of a SLAM scanner georeferenced using GCP. The experiment focused on geodetic work for monitoring earthworks, specifically on surface earth dumps.

Materials and Methods

The experiment was carried out at a landfill site for soil excavated during the construction of a motorway. The reference geodetic network for the tested area was surveyed using a Leica TS60 total station with millimeter accuracy. The reference point cloud was measured using a Leica P40 terrestrial static scanning system. This point cloud was connected to the reference coordinate system using ground control points (GCPs). The tested clouds from the Emesent Hovermap ST-X SLAM scanning system were connected to the reference coordinate system using ground control points provided by targets with reflective foil, and in the second part of the experiment, using trajectory determination by a continuously connected GNSS-RTK receiver mounted on the scanning backpack. The accuracy of the tested scanner was obtained by comparing the reference point cloud with the point clouds determined by the tested scanner.

Experiment Area

The measurements were taken at a soil deposit (Fig. 1) excavated during the construction of the D7 motorway, located in central Bohemia near the town of Slaný. The deposit was approximately 55 m wide, 150 m long, and 15 m high.

Fig. 1. The diagrammatic arrangement of the cyclosizer device

This is a relatively large-scale project, where static measurements are very demanding in terms of the number and connection of stations. If we disregard the possible use of UAVs, the deployment of an easy-to-use SLAM scanner is the ideal option, especially when used without GCPs. The System of the Unified Trigonometrical Cadastral Network coordinate system and the Bpv (Baltic 1957 height) height system, which are mandatory in the Czech Republic, were selected for processing.

The used devices and software

The Leica Nova TS60 total station (Leica Geosystems AG, Switzerland) was used to measure the reference geodetic network. It is the robotic total station manufactured by Leica Geosystems AG, Switzerland (Fig. 4a). The standard deviation of horizontal direction and zenith angle measurements is 0.15 mgon, and the standard deviation of distance measurements is 0.6 mm + 1.0 ppm for the prism and 2 mm + 2 ppm for any arbitrary surface.

Fig. 2 Used devices and aids a) the Leica Nova TS60 robotic total station; b) the Leica ScanStation P40; c) the Emesent Hovermap ST-X with a Trimble R12i GNSS receiver mounted on a backpack; d) a black and white Leica GZT21target on the tribrach; e) a highly reflective target for SLAM data georeferencing on the wooden desk.

The Leica ScanStation P40 (Leica Geosystems AG, Switzerland) is a terrestrial scanner manufactured by Leica Geosystems AG, Switzerland (Fig. 2b). It has a standard deviation of the horizontal and vertical angular measurement of 2.4 mgon and a standard deviation of distance measurement of 1.2 mm + 10 ppm. The scanning

rate is up to 1 million points per second. The range of measured distance is from 0.4 m to 270 m on a surface with a reflectance of 34%. The maximum field of view is 360° × 270°. It is equipped with a liquid dual-axis compensator with an accuracy of 0.45 mgon. The scanner was used to acquire point clouds, serving as a benchmark for the SLAM-acquired point clouds. Each point cloud was georeferenced using four black-and-white targets, with a Leica GZT21 mounted on the tribrach (Fig. 4d). The data were processed using the Leica Cyclone Register 360+ software, version 2023.1.0.

The Emesent Hovermap ST-X is a SLAM scanner manufactured by Emesent Pty Ltd., Australia (Fig. 2c). The LiDAR has 32 channels, with each having a precision of 10 mm. According to manufacturers' specifications (Emesent Pty Ltd., Australia), the mapping accuracy is 15 mm in general environments and 10 mm in indoor and underground environments. The measured distance range is 0.5 m to 300 m. The scanning rate is up to 640,000 points per second (single-return mode) or up to 1.92 million points per second (multi-return mode, up to 3 returns). The field of view is 290°x360°. The weight of the scanner is 1.57 kg. It can be handheld or mounted on a backpack (as in this experiment) or on any other vehicle (ground vehicle, robot, unmanned aerial vehicle). During one part of the measurement, the scanner was connected to the Trimble R12i GNSS receiver using RTK measurement for určení trasy pohybu. The Trimble R12i has a GNSS RTK (Trimble Inc., United States) measurement standard deviation of 8 mm in the horizontal direction and 15 mm in the vertical direction according to the manufacturer's information; in practical applications connected to the CZEPOS network of permanent reference stations, 10 mm and 40 mm. During the second part of the measurement, the scans were georeferenced, and the movement path was corrected using highly reflective 200 mm diameter targets placed on the wooden desk (Fig. 4e). Data were processed using the Emesent Aura software, version 2.0.1.

Measurement and processing of the reference dataset

The reference geodetic network was surveyed using a Leica TS60 total station and the spatial polar method. The measurements were performed using automatic targeting of the Leica GMP111 mini prism. All measurements were performed in two repetitions with independent target levelling. (1st target levelling – targeting of positions I and II, 2nd target levelling – targeting of positions I and II). Four points of the geodetic network defining the experiment's coordinate system (stabilized by wooden pegs) were established in the area around the targeted heap, whose coordinates were determined using the GNSS-RTK method in the S-JTSK and Bpv reference systems. The coordinates of the total station's free station were determined by orientation to these points, from which the coordinates of these orientation points were retroactively determined in order to eliminate random errors in GNSS measurements. The coordinates determined in this way were used to determine other free stations according to current needs. The GCP coordinates for both the Leica P40 and Emesent Hoovermap ST-X scanners were determined twice, with an average difference of 2 mm. The reflective targets for the SLAM scanner were signaled by a Leica GMP 111 mini prism, and the GCPs for the Leica P40 were measured by a direct reflex rangefinder. This determined the coordinates of 15 GCPs for the Leica P40 scanner and 8 GCPs for the Emesent Hovermap ST-X scanner.

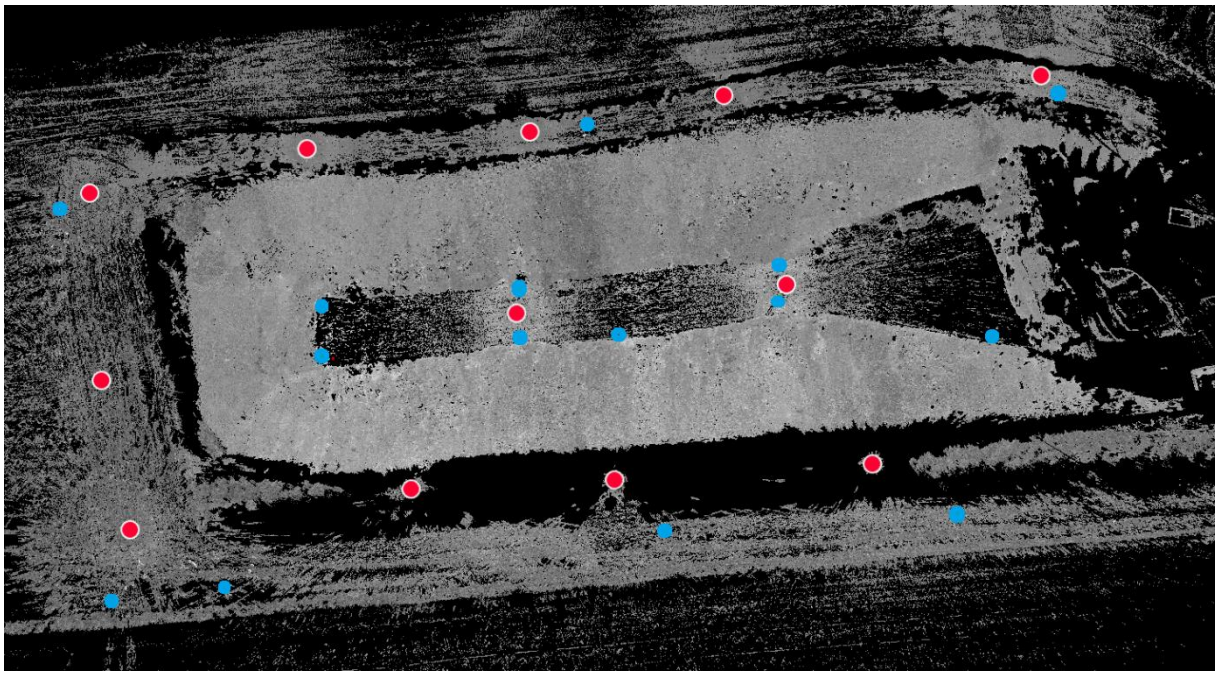

Fig. 3 Stations of P40 scanner (marked in red dots) and positions of GCP (black and white targets, marked in blue dots)

The reference cloud of the site of interest was measured using a Leica P40 scanning system. A total of 12 stations were measured (see Fig. 3, red dots). To combine the individual scans into a single cloud and georeference it, four ad hoc 4.5" Leica GZT21 black-and-white targets were used for each station (see Fig. 2, blue dots). The scanning density was set to 3.1 mm per 10 m. The centers of the targets were acquired by a special scanning procedure during measurement.

Measurement and processing of the Emesent Hovermap ST-X data

Measurements with the tested Emesent Hovermap ST-X scanner were performed according to the manufacturer's recommended procedure. For each measurement, the entire area of interest was surveyed without interruption using a closed measurement loop (Fig. 3). For all measurements, the measuring loop followed roughly the same route, Fig. 5. First, the area was scanned twice without using a GNSS RTK receiver (with subsequent use of eight GCPs, marked with red dots in Fig. 4). Then, the area was scanned twice with a scanner connected online to a Trimble R12i GNSS receiver. A total of four measurements were taken. Each pass took approximately 15 minutes.

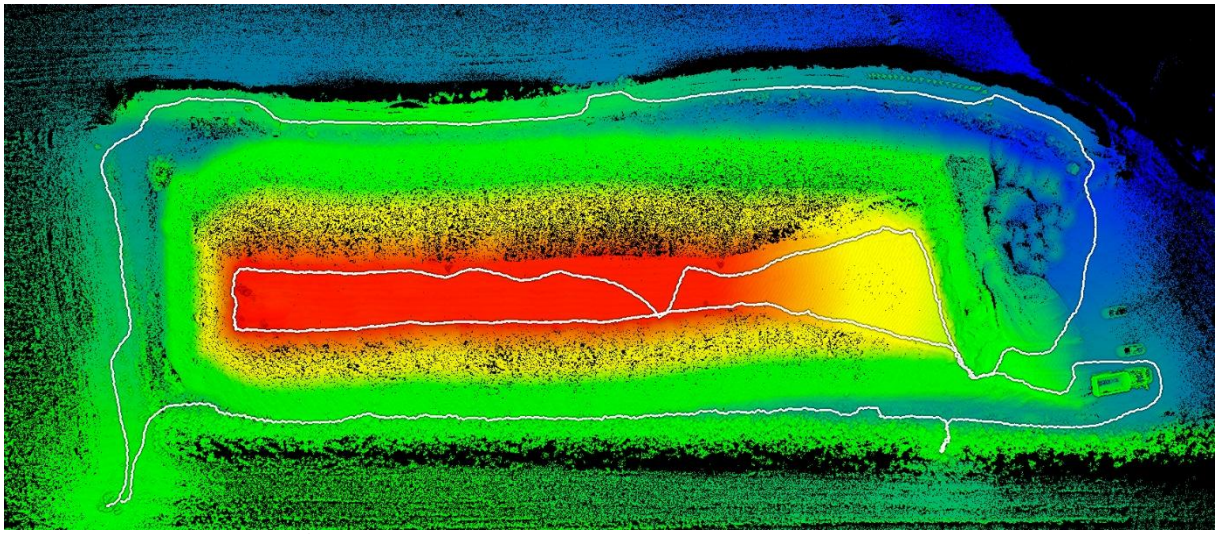

Fig. 3 The path of scanning with Emesent Hovermap ST-X (white color, point cloud colored by the height)

Fig. 4 Positions of the Emesent Hovermap ST-X GCPs (red dots, highly reflective targets – see Fig. 2e)

Basic processing of data acquired by Emesent Hovermap ST-X was performed in Emesent Aura Software ver. 2.0.1. When processing the first two measurements with RTK measurement (RTK_1; RTK_2), EPSG32633

– WGS 84/UTM zone 33N was selected as the target coordinate system in Aura software. The data from this coordinate system was then transformed into the reference coordinate system in the Trimble Business Center software. The reason for this intermediate step was the absence of the correct transformation in the Aura software. In the Czech Republic, GNSS measurements use a transformation to the S-JTSK coordinate system with a Křovák 2018 transformation, which has not yet been implemented in the Aura software.

When processing the second two scans with GCP points (GCP_1; GCP_2), the processing was analogous, with the only difference being that the route was aligned to the automatically identified GCP centers. The accuracies for GCP use were set in the software to 20 mm for GCP detection in the cloud, and 3 mm for the actual accuracy of the GCP coordinates (according to the manufacturer's recommendations).

Determining the accuracy of point clouds

Preprocessing and accuracy assessment were performed using CloudCompare software ver. 2.13.2. A total of four point clouds were obtained in the reference coordinate system. Two were created from GCP points (GCP_1, GCP_2), and two from RTK measurements (RTK_1, RTK_2). All tested point clouds were cropped to match the reference cloud from the P40 scanner. The point clouds were cleaned of vegetation and all other objects not representing the surface of interest (e.g., moving figures, tripods with instruments, etc.).

Because original clouds from SLAM scanning contain a lot of data noise, the obtained clouds were smoothed using the "MLS – Moving least square" function. A search radius of 0.1 m and a polynomial order of 2 were used. This resulted in four additional smoothed point clouds, labeled RTK_1_smooth, RTK_2_smooth, GCP_3_smooth, and GCP_4_smooth, which were also subjected to testing.

The quality of point clouds obtained by SLAM scanning was evaluated by calculating the root mean square deviation (RMSD) between the tested clouds and the reference cloud.

The root mean square error was calculated for each tested pointcloud as:

$$RMSD = \sqrt{\frac{\sum_1^n d_i^2}{n}}, \tag{1}$$

where n is the number of points in the tested point clouds, and di is the smallest distance between the i-th point in the tested poinclouds and the surface which was defined by the reference pointcloud.

The distances were obtained using the function "Compute cloud/cloud distance", which uses k nearest points (in our case, *k* was set to 15) from the reference cloud to create a local triangular irregular network (TIN) and determines the shortest distance between the ith point from the tested cloud and the reference local TIN.

Furthermore, the root mean square errors $RMSD_X$, $RMSD_Y$, and $RMSD_Z$ were calculated by dividing the smallest distances from the previous calculation in the direction of the individual axes:

$$RMSD_X = \sqrt{\frac{\sum_1^n dx_i^2}{n}}, \tag{2}$$

where *n* is the number of points in the tested point clouds and *dx* is the smallest distance between the i-th point in the tested point clouds and the surface, which was defined by the reference point cloud in the direction of the X-axis. From these values, the mean deviation (M_X) and standard deviation (s_X) were then calculated as:

$$M_X = \sqrt{\frac{\sum_1^n dx_i}{n}}, \tag{3}$$

$$s_X = \sqrt{\frac{\sum_1^n (GM - dx_i)^2}{n-1}}, \tag{4}$$

where *n* and dx_i are the same as in the previous calculation. $RMSE_Y$ and $RMSE_Z$ are calculated analogously.

Results

The result of the measurement and processing was a total of 8 point clouds obtained using a SLAM scanner and 1 point cloud (reference) obtained using a static scanner. Their basic characteristics are listed in Table 1.

Regarding the creation of the P40 reference cloud, it should be added that the average standard deviation of the spatial position of the targets during the registration of point clouds was 6 mm.

The calculated RMSD for each measurement is shown in Table 2. The results show that the RMSD from the first RTK measurement is significantly higher than that from the other measurements, which are very similar to

each other. However, considering the accuracy of RTK measurements in the Czech Republic (10 mm in position, 40 mm in height), the results are practically better than expected.

Tab. 1. Basic characteristics of point clouds

Data	Number of points	Mean density [points/m^2]	Approx point spacing [mm]
P40	21 264 635	23459	0,007
GCP_1	23 392 451	22750	0,007
GCP_2	23 593 210	23411	0,007
RTK_1	17 662 236	11214	0,009
RTK_2	17 778 333	9153	0,010

Tab. 2. The resulting RMSDs for each measurement

Data	RMSD - Pass 1 [mm]	RMSD - Pass 2 [mm]	RMSD - Mean [mm]
RTK	25,0	17,5	21,6
GCP	17,4	17,9	17,7
RTK_smooth	23,7	15,5	20,0
GCP_smooth	15,6	15,7	15,7

The manufacturer-declared mapping accuracy (standard deviation, using GCPs) is 15 mm under general conditions and 10 mm indoors, with a local accuracy of 5 mm, which corresponds very well with the results from GCP data. RTK data show slightly worse results, but considering the stated accuracy of the GNSS-RTK receiver, they are also very good. At the same time, a comparison of the original and smoothed data results also shows that only a slight increase in accuracy occurs on the given "rough" surface.

The calculated $RMSD_X$, M_X, s_X, $RMSD_Y$, M_Y, and s_Y for all measurements are shown in Table 3. The results show that the accuracy of the tested clouds along the X and Y axes is similar across all clouds and that, in particular, the clouds are not systematically shifted in either direction along these axes. The residual standard deviations s_X and s_Y are comparable for all measurements.

Tab. 3. The resulting $RMSD_X$, M_X, s_X, $RMSD_Y$, M_Y, and s_Y for each measurement

Data	$RMSD_X$ [mm]	M_X [mm]	s_X [mm]	$RMSD_Y$ [mm]	M_Y [mm]	s_Y [mm]
RTK_1	8,2	0,0	8,2	10,5	-0,2	10,5
RTK_2	7,5	0,6	7,4	9,5	0,0	9,5
GCP_1	6,9	0,0	6,9	8,8	0,1	8,8
GCP_2	7,3	0,0	7,3	9,3	0,0	9,3
RTK_1_smooth	7,9	0,0	7,9	9,9	-0,1	9,9
RTK_2_smooth	6,9	0,5	6,9	8,8	0,1	8,8
GCP_1_smooth	6,5	-0,1	6,5	8,3	0,1	8,3
GCP_2_smooth	6,7	-0,1	6,7	8,5	0,1	8,5

The calculated $RMSD_Z$, M_Z, and s_Z for all measurements are shown in Table 4. These results show that the first RTK measurement is significantly shifted in height, but the shift does not exceed the expected accuracy of height determination using the RTK method. From the above comparison and the contrast between RMSD and average errors M in Table 2 and 3, it is clear that the systematic error mainly affects height, both in RTK and GCP data.

Tab. 4. The resulting $RMSD_X$, M_X, s_X, $RMSD_Y$, M_Y, and s_Y for each measurement

Data	$RMSD_Z$ [mm]	M_Z [mm]	S_Z [mm]
RTK_1	8,2	0,0	8,2
RTK_2	7,5	0,6	7,4
GCP_1	6,9	0,0	6,9
GCP_2	7,3	0,0	7,3
RTK_1_smooth	7,9	0,0	7,9
RTK_2_smooth	6,9	0,5	6,9
GCP_1_smooth	6,5	-0,1	6,5
GCP_2_smooth	6,7	-0,1	6,7

Due to the thickness of the original point clouds, it is not illustrative to present their deviations on them; therefore, in Figures 5 and 6, the deviations of the smoothed clouds relative to the reference P40 point cloud are presented in the main text. Other graphical presentations of the results are in the appendices.

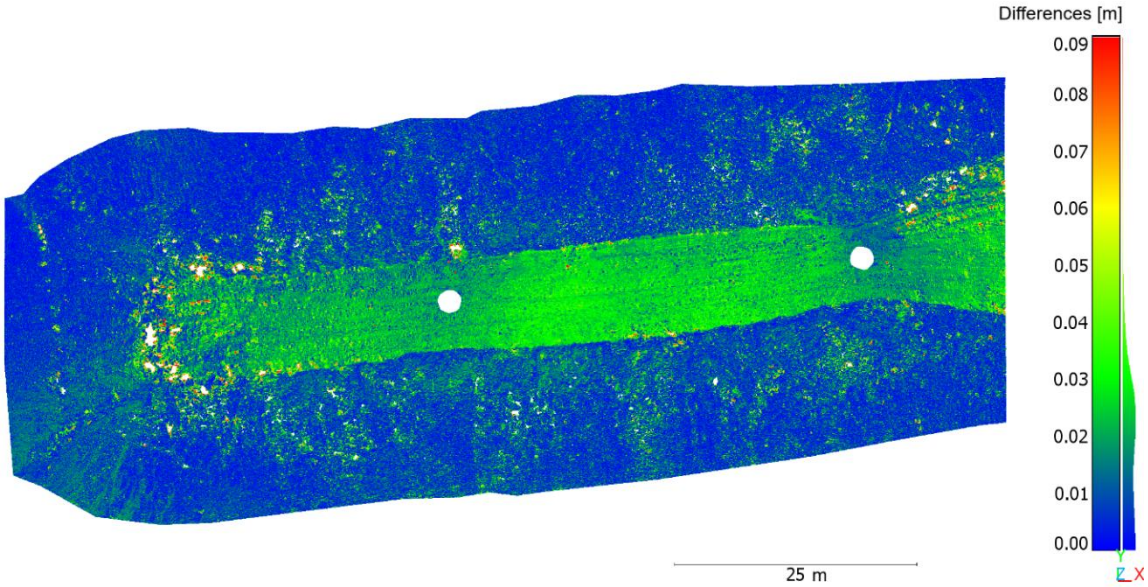

Fig. 5 Distribution of deviations of the tested point cloud RTK_1_smooth relative to the reference point cloud P40 – RMSD 25 mm

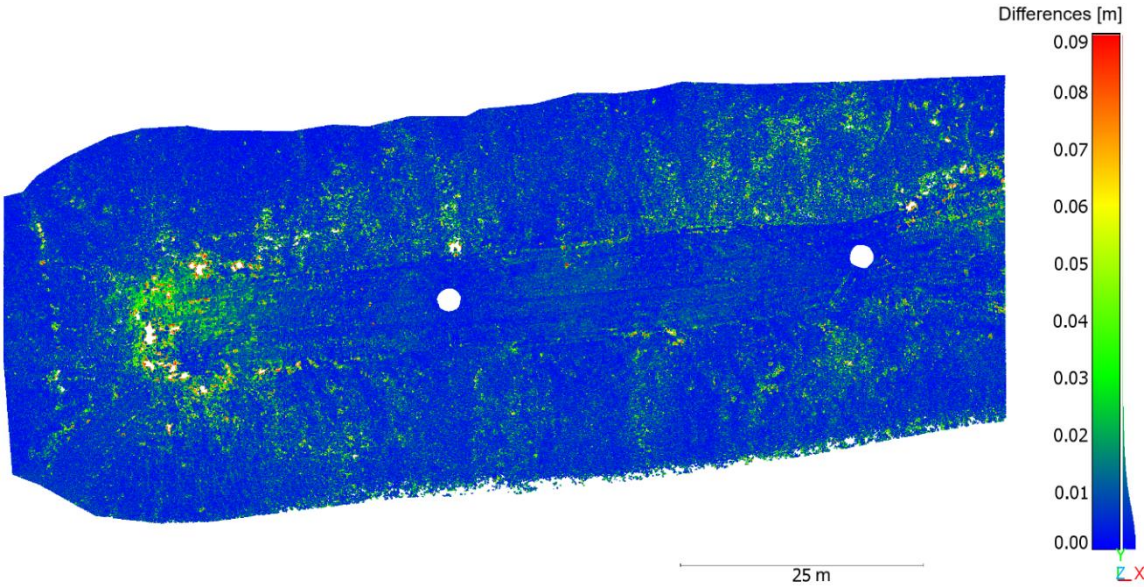

Fig. 6 Distribution of deviations of the tested point cloud GCP_1_smooth relative to the reference point cloud P40 – RMSD 16 mm

Discussion

SLAM scanning is an exceptionally suitable method for ground monitoring of earthworks, as static scanning requires the use of a large number of positions. When using SLAM technology, it is sufficient to scan the monitored area on foot, and the virtually infinite number of positions in a large part of the unscanned area (obstructions) common in static scanning are not necessary. An alternative to SLAM scanning is UAV scanning, which, however, requires a pilot's license and, depending on the country, various permits. This article presents an experiment whose results are used to test the possibility of this specific application, as SLAM technology requires objects and shapes in the scanned scene that allow for ideal unambiguous orientation in order to compose a point cloud, which is usually the case in interiors and man-made structures, but less so in the case of natural shapes, and are also more or less covered by chaotic vegetation. At the same time, the aim of the experiment was to determine whether this type of work could be carried out without GCP, thereby further simplifying the measurement process.

For the SLAM scanning system itself, Emesent Hoovermap ST-X, the manufacturer specifies a mapping accuracy of 15 mm (RMSD), which was not achieved in our experiment. Figure 10 may help with a more in-depth analysis, where it is clear that there are significant differences between the slopes of the heap and the top. The explanation can be found in Fig. 5, where the movement route shows access to the top of the heap via a single narrow path (bottom right in the figure). There is no other connection between the point clouds of the top and sides of the heap, as it is not possible to see from the top to the sides or from the bottom to the top.

Numerically, this explanation can be substantiated by the average height deviations of the separate clouds TOP and SIDES, where for the top part of the RTK_1 data, the mean deviation is M_{TOP_Z,RTK_1} = -22 mm, but for the sides part M_{SIDES_Z,RTK_1} = - 3 mm – here we are actually dealing with two "separate" clouds. Similarly, although not as extreme, for RTK_2 data, $M_{TOP\_Z,\ RTK\_2}$ = -7 mm, but $M_{SIDES\_Z,\ RTK\_2}$ = +2 mm. Here, the difference is not as striking, but still obvious. In the case of GCP clouds, the result also indicates that the sides and top of the heap are not perfectly connected, even though two GCPs are stabilized (not optimally) at the top of the heap. For both GCP_1 and GCP_2 data, the results are identical: $M_{TOP\_Z,\ GCP}$ = -8 mm, and $M_{SIDES\_Z,\ GCP}$ = -1 mm.

This suggests the need to consider bottlenecks in connecting areas and the placement of GCPs when reconnoitering and planning a route. In our presented experiment, we placed only two GCPs on top of the heap, approximately in the middle and on one side of the area (see fig. 3). Based on our findings, it would be ideal to place four GCPs at the corners of the upper area. If the systematic shift at the top of the heap were eliminated, the manufacturer's specified accuracy would certainly be achieved. The problem could probably also be solved by having the scan route run directly along the edge of the top part, but this was not feasible here due to operator safety concerns.

Comparing the accuracy of RTK_1/2 and GCP_1/2 data when the systematic shifts explained above is relatively simple – in terms of position, both methods are practically equivalent (which is due to the positional accuracy of GNSS-RTK measurements – approx. 10 mm), but a larger shift may occur in the determination of height due to the current GNSS-RTK measurement, so it would be advisable to connect this measurement to at least one known height and, if necessary, correct the height of the entire point cloud for the systematic error detected.

Conclusions

An experiment was conducted to test the use of the Emesent Hoovermap ST-X SLAM scanner for monitoring earthworks, specifically mapping a soil pile measuring approximately 150 m x 55 m x 15 m. The aim was to experimentally determine and compare the accuracy of two measurement methods – using georeferencing and route adjustment using GCP, and using onboard GNSS-RTK. The result confirms the suitability of both methods, with a total RMSD of less than or equal to 25 mm, which is definitely sufficient for this type of surveying work. During the measurement itself, it is advisable to emphasize the correct placement of GCPs, taking into account the need to ensure reliable georeferencing of each area that may not be reliably connected to others (in this case, the top of the heap). For the GNSS RTK measurement variant, which at first glance is easier and faster because there is no need to stabilize and target GCPs, it is definitely recommended to check and rectify heights using as few control points as possible due to the potential overall systematic height shift.

References

Antova, G. (2024). Portable laser scanning solutions for 3D modelling of large buildings. ˜the œInternational Archives of the Photogrammetry, Remote Sensing and Spatial Information Sciences/International Archives of the Photogrammetry, Remote Sensing and Spatial Information Sciences, XLVIII-4/W10-2024, 13–19. https://doi.org/10.5194/isprs-archives-xlviii-4-w10-2024-13-2024

Bartmiński, P., Siłuch, M., & Kociuba, W. (2023). The effectiveness of a UAV-Based LIDAR survey to develop digital terrain models and topographic texture analyses. Sensors, 23(14), 6415. https://doi.org/10.3390/s23146415

Běloch, L., & Pavelka, K. (2025). Low-Cost solution for kinematic mapping using spherical camera and GNSS. *Applied Sciences*, *15*(11), 5972. https://doi.org/10.3390/app15115972

Del Carmen Vílchez-Lara, M., Molinero-Sánchez, J. G., Rodríguez-Moreno, C., Gómez-Blanco, A. J., Reinoso-Gordo, J. F., Del Carmen Vílchez-Lara, M., . . . Reinoso-Gordo, J. F. (2024). High Resolution 3D Model of Heritage Landscapes Using UAS LiDAR: The Tajos de Alhama de Granada, Spain. Land, 13(1), 75. https://doi.org/10.3390/land13010075

Dragomir, L. O., Popescu, C. A., Herbei, M. V., Popescu, G., Herbei, R. C., Salagean, T., Bruma, S., Sabou, C. & Sestras, P. (2025). Enhancing Conventional Land Surveying for Cadastral Documentation in Romania with UAV Photogrammetry and SLAM. Remote Sensing, 17(13), 2113. https://doi.org/10.3390/rs17132113

Eker, R., Ucar, Z., & Aydın, A. (2022). A PRIMARY TEST RESULTS OF a HANDHELD MOBILE LASER SCANNER IN EXTRACTION OF TREE PARAMETERS. The International Archives of the Photogrammetry, Remote Sensing and Spatial Information Sciences/International Archives of the Photogrammetry, Remote Sensing and Spatial Information Sciences, XLIII-B1-2022, 207–212. https://doi.org/10.5194/isprs-archives-xliii-b1-2022-207-2022

Emmanouil, T., Maria, P., Kerasiotis, A., Saer, A. E., & Grammatikopoulos, L. (2025). A Comparative Assesment of Lidar Slam Accuracy Using TLS Data. In 2025 6th International Conference in Electronic Engineering

Information Technology (EEITE) (pp. 1–5). 2025 6th International Conference in Electronic Engineering Information Technology (EEITE). IEEE. https://doi.org/10.1109/eeite65381.2025.11166016

Flener, C., Vaaja, M., Jaakkola, A., Krooks, A., Kaartinen, H., Kukko, A., Kasvi, E., Hyyppä, J. & Alho, P. (2013). Seamless mapping of river channels at high resolution using mobile LIDAR and UAV-Photography. *Remote Sensing*, *5*(12), 6382–6407. https://doi.org/10.3390/rs5126382

Fortuna, S., Chiodini, S., Valmorbida, A., & Pertile, M. (2025). Comparative analysis of LiDAR-SLAM systems: A study of a motorized optomechanical LIDAR and an MEMS scanner LiDAR. Sensors, 25(17), 5352. https://doi.org/10.3390/s25175352

Gharebaghi, A., Mostafavi, M. A., Larouche, C., Esmaeili, K., & Genon, M. (2021). Precise indoor localization and mapping using mobile laser scanners: a scoping review. *GEOMATICA*, *75*(4), 1–13. https://doi.org/10.1139/geomat-2021-0011

Chen, P., Zhao, X., Zeng, L., Liu, L., Liu, S., Sun, L., Li, Z., Chen, H., Liu, G., Qiao, Z., Qu, Y., Xu, D., Li, L. & Li, L. (2025). A review of research on SLAM technology based on the fusion of LiDAR and Vision. Sensors, 25(5), 1447. https://doi.org/10.3390/s25051447

Chrbolková, A., Štroner, M., Urban, R., Michal, O., Křemen, T., & Braun, J. (2025). A comparative study of indoor accuracies between SLAM and static scanners. *Applied Sciences*, *15*(14), 8053. https://doi.org/10.3390/app15148053

Chudá, J., Výbošťok, J., Tomaštík, J., Chudý, F., Tunák, D., Skladan, M., Tuček, J. & Mokroš, M. (2024). Prompt Mapping Tree Positions with Handheld Mobile Scanners Based on SLAM Technology. *Land*, *13*(1), 93. https://doi.org/10.3390/land13010093

Issaoui, A. E., Feng, Z., Lehtomäki, M., Hyyppä, E., Hyyppä, H., Kaartinen, H., Kukko, A. & Hyyppä, J. (2021). Feasibility of Mobile Laser Scanning towards Operational Accurate Road Rut Depth Measurements. *Sensors*, *21*(4), 1180. https://doi.org/10.3390/s21041180

Janus, J., & Ostrogórski, P. (2022). Underground Mine Tunnel Modelling Using Laser Scan Data in Relation to Manual Geometry Measurements. Energies, 15(7), 2537. https://doi.org/10.3390/en15072537

Jiang, L., Luan, J., Dong, Y., Ren, Y., Pan, Y., Zeng, X., Wei, M., Long, S., Yuan, J., Xiang, X. & Ge, X. (2024). Accuracy analysis and efficiency evaluation of 3D laser scanning technology based on SLAM in underground mine roadway measurement. *Highlights in Science Engineering and Technology*, *105*, 82–90. https://doi.org/10.54097/2zae2736

Kalenjuk, S., & Lienhart, W. (2022). A method for efficient quality control and enhancement of mobile laser scanning data. *Remote Sensing*, *14*(4), 857. https://doi.org/10.3390/rs14040857

Koszyk, J., Łabędź, P., Grzelka, K., Jasińska, A., Pargieła, K., Malczewska, A., Strząbała, K., Michalczak, M. & Ambroziński, Ł. (2023). EVALUATION OF LIDAR ODOMETRY AND MAPPING BASED ON REFERENCE LASER SCANNING. The International Archives of the Photogrammetry, Remote Sensing and Spatial Information Sciences/International Archives of the Photogrammetry, Remote Sensing and Spatial Information Sciences, XLVIII-1/W3-2023, 79–84. https://doi.org/10.5194/isprs-archives-xlviii-1-w3-2023-79-2023

Kovanič, Ľ. (2013). Possibilities of Terrestrial Laser Scanning Method in Monitoring of Shape Deformation in Mining Plants. *Inż. Miner. J. Pol. Miner. Eng. Soc., 1*, 29–41.

Kovanič, Ľ., Peťovský, P., Topitzer, B., & Blišťan, P. (2024). Complex Methodology for Spatial Documentation of Geomorphological Changes and Geohazards in the Alpine Environment. *Land*, *13*(1), 112. https://doi.org/10.3390/land13010112

Kovanič, Ľ., Peťovský, P., Topitzer, B., Blišťan, P., & Tokarčík, O. (2025). Analysis of the qualitative parameters of mobile laser scanning for the creation of cartographic works and 3D models for digital twins of urban areas. *Applied Sciences*, *15*(4), 2073. https://doi.org/10.3390/app15042073

Kovanič, Ľ., Peťovský, P., Topitzer, B., Blišťan, P., & Tokarčík, O. (2025b). Qualitative Assessment of Point Cloud from SLAM-Based MLS for Quarry Digital Twin Creation. *Applied Sciences*, *15*(22), 12326. https://doi.org/10.3390/app152212326

Křemen, T., Michal, O., Jiřikovský, & T. Kuric, I. (2024). Long-distance SLAM scanning of mine tunnel - testing of precision and accuracy of Emesent Hovermap ST-X. *Acta Montanistica Slovaca*, *29*(v29/i3), 630–642. https://doi.org/10.46544/ams.v29i3.10

Liu, J., Azhar, S., Willkens, D., & Li, B. (2023). Static Terrestrial Laser Scanning (TLS) for Heritage Building Information Modeling (HBIM): A Systematic review. Virtual Worlds, 2(2), 90–114. https://doi.org/10.3390/virtualworlds2020006

Maset, E., Matellon, A., Gubiani, S., Visintini, D. & Beinat, A. (2025). Introducing SLAM-Based portable laser scanning for the metric testing of topographic databases. *Remote Sensing*, *17*(19), 3316. https://doi.org/10.3390/rs17193316

Muhojoki, J., Hakala, T., Kukko, A., Kaartinen, H. & Hyyppä, J.(2024). Comparing positioning accuracy of mobile laser scanning systems under a forest canopy. Science of Remote Sensing, 9, 100121. https://doi.org/10.1016/j.srs.2024.100121

Pei, J., Yao, C., Deng, Z., Ren, Z., & Yang, Y. (2021). The application of 3D laser scanning and unmanned ship sounding in the reexamination of reservoir storage capacity. *IOP Conference Series Earth and Environmental Science*, *719*(4), 042052. https://doi.org/10.1088/1755-1315/719/4/042052

Pukanská, K., Bartoš, K., Gašinec, J., Pašteka, R., Zahorec, P., Papčo, J., Bella, P., Andrássy, E., Dušeková, L., Bobíková, D. & Kseňak, Ľ. (2024). Methodological approaches to survey complex ice cave environments - the case of Dobšiná (Slovakia). Frontiers in Environmental Science, 12. https://doi.org/10.3389/fenvs.2024.1484169

Rocha, G., Mateus, L., & Ferreira, V. (2024). Historical Heritage Maintenance via Scan-to-BIM Approaches: A case study of the Lisbon Agricultural Exhibition Pavilion. ISPRS International Journal of Geo-Information, 13(2), 54. https://doi.org/10.3390/ijgi13020054

Singh, S. K., Banerjee, B. P., & Raval, S. (2022). A review of laser scanning for geological and geotechnical applications in underground mining. International Journal of Mining Science and Technology, 33(2), 133–154. https://doi.org/10.1016/j.ijmst.2022.09.022

Štroner, M., Urban, R., Křemen, T., Braun, J., Michal, O., & Jiřikovský, T. (2024). Scanning the underground: Comparison of the accuracies of SLAM and static laser scanners in a mine tunnel. *Measurement*, *242*, 115875. https://doi.org/10.1016/j.measurement.2024.115875

Szrek, A., Romańczukiewicz, K., Kujawa, P., & Trybała, P. (2024). Comparison of TLS and SLAM technologies for 3D reconstruction of objects with different geometries. *IOP Conference Series Earth and Environmental Science*, *1295*(1), 012012. https://doi.org/10.1088/1755-1315/1295/1/012012

Urban, R., Štroner, M., Braun, J., Suk, T., Kovanič, Ľ., & Blistan, P. (2024). Determination of Accuracy and Usability of a SLAM Scanner GeoSLAM Zeb Horizon: A Bridge Structure Case Study. *Applied Sciences*, *14*(12), 5258. https://doi.org/10.3390/app14125258

Appendices

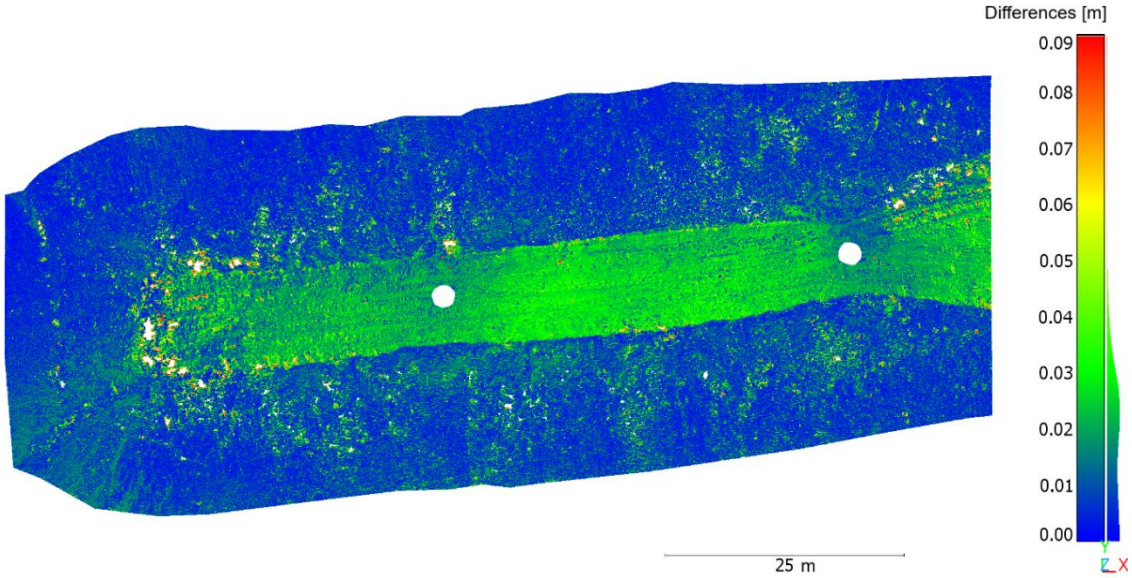

Fig. A1 Distribution of deviations of the tested point cloud RTK_1_smooth relative to the reference point cloud P40

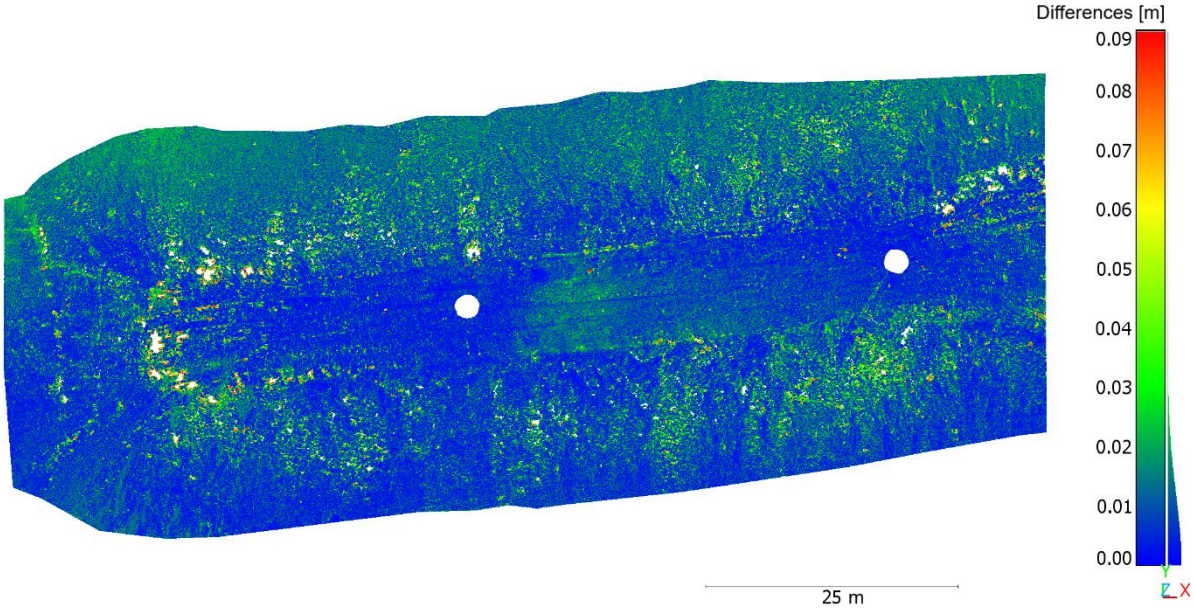

Fig. A2 Distribution of deviations of the tested point cloud RTK_2_smooth relative to the reference point cloud P40

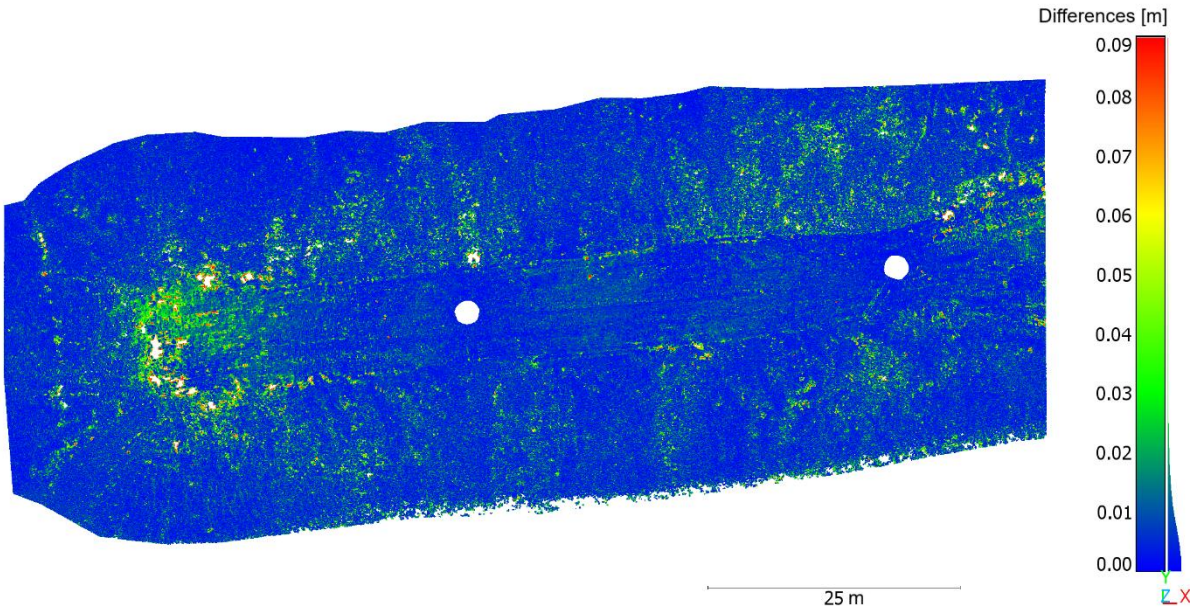

Fig. A3 Distribution of deviations of the tested point cloud GCP_1_smooth relative to the reference point cloud P40

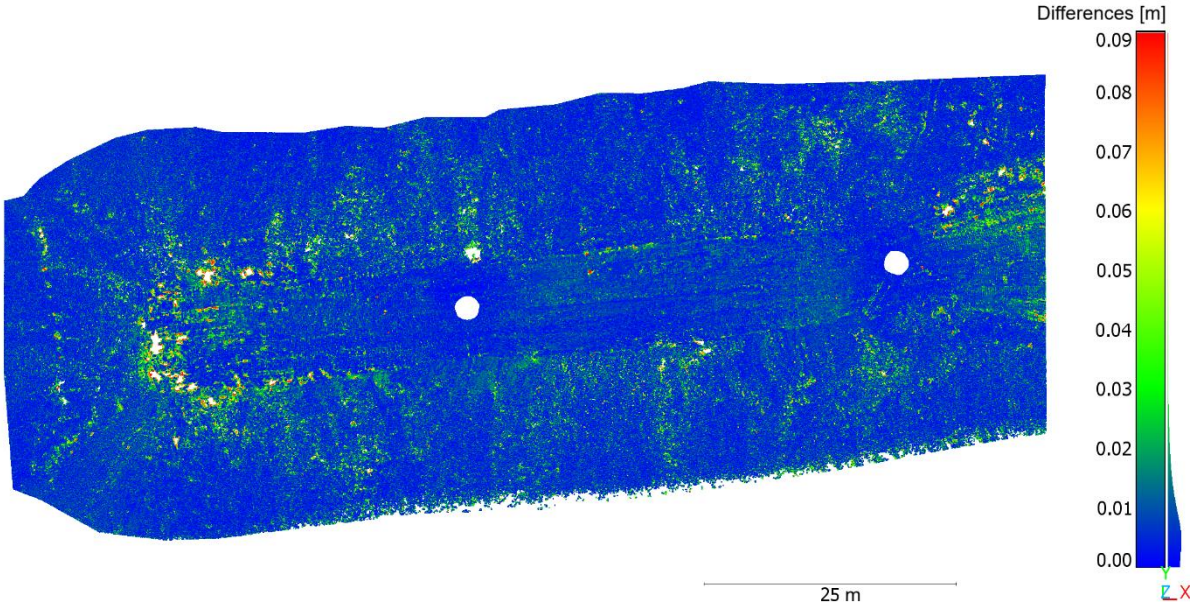

Fig. A4 Distribution of deviations of the tested point cloud GCP_2_smooth relative to the reference point cloud P40